Advances in Concrete Construction, *Vol. 9, No. 6 (2020) 597-610*
DOI: https://doi.org/10.12989/acc.2020.9.6.597

Preload effects on behaviour of FRP confined concrete: Experiment, mechanism and modified model

Vui Van Cao*[1,2]

[1]*Faculty of Civil Engineering, Ho Chi Minh City University of Technology (HCMUT), 268 Ly Thuong Kiet Street, District 10, Ho Chi Minh City, Vietnam*
[2]*Vietnam National University at Ho Chi Minh City (VNU-HCM), Linh Trung Ward, Thu Duc District, Ho Chi Minh City, Vietnam*

(*Received March 15, 2019, Revised May 8, 2020, Accepted May 29, 2020*)

Abstract. Stress-strain models of fibre reinforced polymer (FRP) confined concrete have been widely investigated; however, the existing load which is always supported by structures during the retrofitting phase, namely 'preload', has been neglected. Thus, preload effects should be clarified, providing insightful information for FRP retrofitting of structures with preload conditions. Towards this aim, experiments were performed for 27 cylinder concrete specimens with the diameter 150 mm and the height 300 mm. Three specimens were used to test the compressive strength of concrete to compute the preloads 20%, 30% and 40% of the average strength of these specimens. Other 24 specimens were divided into 2 groups; each group included 4 subgroups. Four subgroups were subjected to the above preloads and no preload, and were then wrapped by 2 FRP layers. Similar designation is applied to group 2, but wrapped by 3 FRP layers. All specimens were tested under axial compression to failure. Explosive failure is found to be the characteristic of specimens wrapped by FRP. Experimental results indicated that the preload decreases 12-13% the elastic and second stiffness of concrete specimens wrapped by 2 FRP layers. The stiffness reduction can be mitigated by the increase of FRP layers. Preload negligibly reduces the ultimate force and unclearly affects the ultimate displacement probably due to complicated cracks developed in concrete. A mechanism of preload effects is presented in the paper. Finally, to take into account preload effects, a modification of the widely used model of un-preload FRP confined concrete is proposed and the modified model demonstrated with a reasonable accuracy.

Keywords: preload; FRP; confinement; strengthening; compression; force-displacement relationship

1. Introduction

The advanced fibre reinforced polymer (FRP) materials with their distinct properties such as high strength, lightweight and ease of application, provide appropriate retrofitting solutions for a huge demand of retrofitting or upgrading existing structures around the world. Compared with many retrofitting methods such as using steel braces and enlarging structural members, FRP retrofitting does not occupy the living space or does not change the architecture of buildings. The applications of FRP are diverse such as flexural strengthening (Sumathi and Arun 2017), shear strengthening (Abdel-Kareem 2014), confinement (Cao and Pham 2019, Eslami and Ronagh 2013, Hosseinpour and Abbasnia 2014, Hosseinpour and Abdelnaby 2015, Mesbah and Benzaid 2017), or combinations (Norris *et al.* 1997). In addition, FRP has demonstrated to be an appropriate material for repairing concrete (Ahmad *et al.* 2018), reinforced concrete (RC) members (Lao *et al.* 2019, Mesbah and Benzaid 2017, Ozcan *et al.* 2010, Saadatmanesh *et al.* 1997) or RC structures (Balsamo *et al.* 2005) which were previously damaged.

Regarding the confinement retrofitting, FRP wraps provide a favourable condition for concrete; consequently, properties of concrete such as strength and ductility significantly increase as confirmed by researchers (Harajli *et al.* 2006, Lam and Teng 2003a, b, Wei and Wu 2012, Wu *et al.* 2007, Youssef *et al.* 2007). FRP wrapping is considered to be a suitable retrofitting solution for structures poorly-confined due to deficiencies of transverse reinforcement (Cao and Pham 2019, Cao and Ronagh 2014, Eslami and Ronagh 2013). Compared with the confinement of transverse reinforcement, FRP confinement exhibits many advantages such as stronger confinement for the whole cross section. Thus, FRP confined columns exhibits much higher energy absorption capability (Harajli and Rteil 2004, Sheikh and Yau 2002), strength and ductility (Rahai and Akbarpour 2014, Sheikh and Yau 2002) than columns confined by steel stirrups. At the macro level of frame structures, FRP confinement significantly improves the seismic capacity of the original frame as reported in experimental (Balsamo *et al.* 2005, Garcia *et al.* 2010, Ludovico *et al.* 2008a, Ludovico *et al.* 2008b) and numerical (Eslami and Ronagh 2013, Mortezaei *et al.* 2010) studies. FRP confinement results in higher deformation capacity (Ludovico *et al.* 2008a) and less damage (Cao and Ronagh 2014, Ludovico *et al.* 2008a) of the retrofitted frame than the original frame.

Numerous studies have been performed for concrete confined by FRP. Many stress-strain models of FRP confined concrete were proposed (Harajli *et al.* 2006, Lam

*Corresponding author, Associate Professor
E-mail: cvvui@hcmut.edu.vn

ISSN: 2287-5301 (Print), 2287-531X (Online)

and Teng 2003a, b, Wei and Wu 2012, Wu *et al.* 2007, Youssef *et al.* 2007) and, thus, are helpful to predict the behaviour of RC structures (Eslami and Ronagh 2013, Mortezaei *et al.* 2010). In these stress-strain models of FRP confined concrete, effects of existing loads (permanent dead load such as self-weight of structures and part of live load) supported by structures during the retrofitting phase, namely 'preload', are neglected. However, in practice, preload always exists and is inevitable before and during the retrofitting phase. The preload caused initial stress and deformation in concrete before the FRP confinement becomes effective, leading to different stress-strain behaviour compared with the case without preload. Without fully understanding the effects of preload, designers may feel uncomfortable on their design when limited information of this issue can be found in literature. Therefore, the preload effects on properties and behaviour of FRP-confined concrete should be investigated.

To the author's knowledge, preload effects on retrofitted columns were addressed in a limited number of studies as reviewed in the following. Takeuti *et al.* (2008) experimentally evaluated the preload effects of on RC columns strengthened by high-strength concrete jackets and concluded that preload might not cause detrimental effect on the load-carrying capacity of jacketed columns; however, it could increase the deformability. Vandoros and Dritsos (2006, 2008) investigated the effects of axial preload on concrete columns strengthened by concrete jackets. Their results showed the positive effects of preload on increasing the load-carrying and deformation capacity but reducing the initial stiffness. Papanikolaou *et al.* (2013) performed an analytical study on preload effects on jacketed RC columns and concluded that the axial preload has marginally favorable effect on flexural strength. In addition, the preload effects of become noticeable in cases of high axial compression but not in case of low compression. Pan *et al.* (2017b) tested 32 preloaded circular concrete specimens (diameter 110 mm and height 200 mm) and 16 preloaded square specimens (100 mm×100 mm×200 mm) confined by CFRP with consideration of different preload ratios varying from 0.3 to 0.8. Before applying FRP wraps, square specimens were rounded at corners with the radius 20 mm. Their test results showed that, with the preload ratio less than 0.6 regardless the section shape, the stress-strain curve is lower and the modulus of the second branch is smaller than those in case without preload. These results were explained by that micro crack of preloaded concrete is higher and the lateral confinement of FRP in preloaded specimens is lower than that of un-preloaded specimens when concrete has similar lateral strain. Based on the experimental results, Pan *et al.* (2017b) proposed theoretical models to predict the behaviour of preloaded concrete confined by FRP. It is worth noting that, they clearly stated that the theoretical models were developed based on the results of small diameter specimens and they encouraged further experimental studies on larger-scale specimens to improve the understanding on the behaviour of preloaded concrete confined by FRP wraps. Pan *et al.* (2017a) used the test results to develop a new failure surface theory and a new analysis-oriented model. They concluded that the preload decreased the strength and strain capacity of FRP-onfined concrete and these became more pronounce when the preload ratio increases because of the micro crack in concrete and the tensile strain lag in FRP. The authors found the different effects of number of FRP layers on the behaviour of FRP confined concrete with preload and stated that further tests on this issue should be carried out. Ferrotto *et al.* (2018) used a modified analysis-oriented stress-strain model to analyse the compressive behaviour of circular preloaded concrete columns wrapped by FRP. They concluded that preload reduced the secant stiffness because the preload resulted in lower confinement level. Recently, Sathwik *et al.* (2019) conducted an experiment on 6 CFRP wrapped and 3 plain concrete cylinder specimens with diameter of 100 mm and the height of 200 mm. These 6 CFRP wrapped specimens were divided into three groups which were loaded to 0% (un-preload), 50% and 70% the strength of plain concrete specimens, and then wrapped by 1 FRP layer. These specimens were tested and numerical models using ABAQUS were developed. The experimental and numerical results showed that, the strength of FRP confined concrete decreased 11.6% and 13.6% due to the preload 50% and 70%, respectively.

Amongst the aforementioned relatively limited research, only 4 studies (Ferrotto *et al.* 2018, Pan *et al.* 2017a, Pan *et al.* 2017b, Sathwik *et al.* 2019) directly addressed the effects of preload on concrete confined by FRP, and further investigation on this area should be thus conducted, as encouraged by previous researchers (Pan *et al.* 2017b), to help structural engineers have additional better understanding on retrofitting structures. This current paper aims at the preload effects on mechanical properties and behaviour of FRP confined concrete. To achieve this aim, experiments on 27 concrete cylinder specimens with the diameter of 150 mm and the height of 300 mm, with and without preload and FRP wraps subjected to axial compression were conducted. Conclusions were made based on analyses of the experimental results. In addition, a mechanism to explain the preload effects of on behaviour of FRP confined concrete is presented. Finally, a modification to the available model to take into account the preload effects of FRP confined concrete is proposed.

2. Experimental program

2.1 Materials and specimens

Composition per m^3 of concrete included 0.880 m^3 stone aggregate D_{max} 22 mm, 0.475 m^3 river sand 0-4 mm as fine aggregate, 327 kg of cement PC 40 and 185 litres of water. The thickness of a CFRP layer is 0.167 mm. Six specimens of FRP, labeling '1' to '6' (Fig. 1(a)) were tested to failure as shown in Fig. 1(b). The average tensile strength and elastic modulus were 3629.6 MPa and 235863.6 MPa, respectively.

Fig. 2 shows 27 specimens used for the experiments in this current study. The diameter of specimens was 150 mm and height was 300 mm. The specimens in the front row are without preload, including 3 plain concrete specimens (to test the compressive strength of concrete), 3 specimens wrapped by 2 FRP layers and 3 specimens wrapped by 3

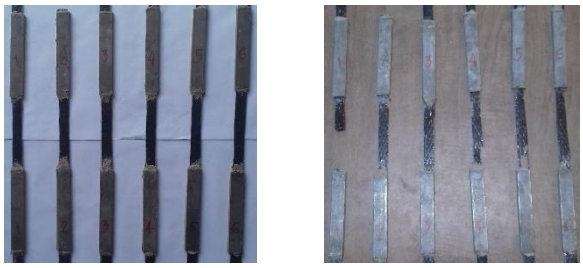

(a) Specimens before testing (b) Specimen after testing

Fig. 1 Plat coupon tensile tests

Fig. 2 Specimens

FRP layers. The specimens in the second and the third rows were firstly loaded to their designed preloads and then wrapped by CFRP. Nine specimens in the second row were wrapped by 2 FRP layers while nine specimens in third row are wrapped by 3 FRP layers. The names of specimens were formulated as 'nL-m%-i', in which, 'nL' is the number of FRP layers, 'm%' is the preload percentage and 'i' is the specimen number. Table 1 shows detailed information of 27 cylinder specimens with classifications into groups based on the number of layers and subgroups based the preload percentage.

The average compressive load of the three plain concrete cylinder specimens at the age of 28 days was 487 kN, and thus the compressive strength was 27.56 MPa. The axial strain at maximum stress was 0.0025. The axial preload applied in this study is based on the values used by Liew and Xiong (2009) who computed that the preload was 20-30% and they used 30% in their experiment. In this current study, the preload on concrete specimens prior to FRP wrapping was 20%, 30% and 40%, which were the percentage of the preload to the load-carrying capacity of plain concrete specimens (487 kN); consequently, the preload of 97.4 kN, 146.1 kN and 194.8 kN were used, as shown in the third column of Table 1.

The preload mechanism is worth describing herein. Two steel bolts with diameter 22 mm and two steel plates with the thickness of 18 mm were used to create preload for specimens. Fig. 3 illustrates the preload system, in which the specimen was preloaded by two bolts located symmetrically to the centre line of specimen. The diameter of holds was 26 mm which is larger than that of bolts (22 mm) to release the preload when the axial force is larger than the preload. Fig. 3(a) shows the specimen under preload by fastening the bolts. The tension forces in these bolts were controlled by a torque wrench used during the fastening phase. The torque wrench allows for setting the

Table 1 Details of the tested specimens

No.	Name	Preload (kN)	Subgroup	Note
1	0L-0%-1			
2	0L-0%-2	0		Plain concrete specimens
3	0L-0%-3			
4	2L-0%-1			
5	2L-0%-2	0	2L-0	
6	2L-0%-3			
7	2L-20%-1			
8	2L-20%-2	94.7	2L-20	
9	2L-20%-3			Group 1: specimens wrapped by 2 FRP layers
10	2L-30%-1			
11	2L-30%-2	146.1	2L-30	
12	2L-30%-3			
13	2L-40%-1			
14	2L-40%-2	194.8	2L-40	
15	2L-40%-3			
16	3L-0%-1			
17	3L-0%-2	0	3L-0	
18	3L-0%-3			
19	3L-20%-1			
20	3L-20%-2	94.7	3L-20	
21	3L-20%-3			Group 2: specimens wrapped by 3 FRP layers
22	3L-30%-1			
23	3L-30%-2	146.1	3L-30	
24	3L-30%-3			
25	3L-40%-1			
26	3L-40%-2	194.8	3L-40	
27	3L-40%-3			

torsional moment applied to the fastener which creates a targeted tension force to the sharks. The friction between the fasteners and the steel plate was minimised by oil to increase the accuracy. The tension force in each bolt was half of the designed preload on specimen. After preloading, these specimens were then wrapped by two and three FRP layers. After 3 weeks, CFRP retrofitted specimens were tested to failure. Subjected to loading from the hydraulic jack during the compression tests, the bolts were automatically deactivated when the applied axial load was larger than the preload as illustrated in Fig. 3(b).

2.2 Test setup

Fig. 4(a) shows the outline of the experiment setup while Fig. 4(b) shows a specimen on the testing machine. The capacity of the hydraulic jack is 3000 kN. After installing specimens into the testing position, specimens were covered by a steel mesh as can be seen in Fig. 4(b) to avoid concrete debris shooting when specimens failed. The axial displacement was simultaneously measured by two linear variable displacement transducers (LVDT) which were positioned at the two opposite sides of specimens. These LVDTs and the load cell were connected to data logger TDS 601-A and computer system. Firstly, the specimens were loaded to 50 kN and released to close to zero to eliminate errors due to contacting. The specimen was then loaded to failure. The axial force and

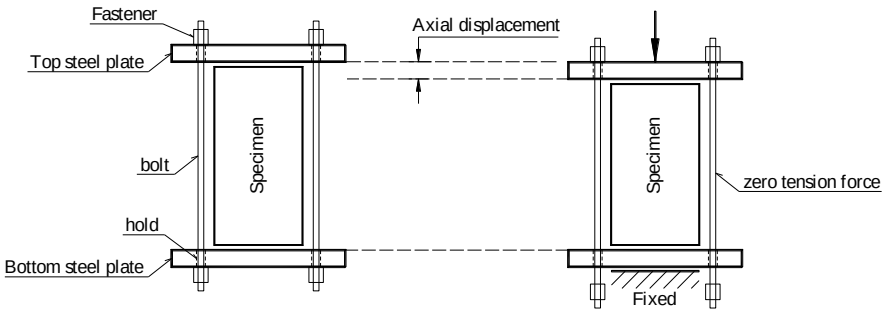

(a) Specimen under preload (b) Specimen under loading to failure

Fig. 3 Preload system for concrete specimens

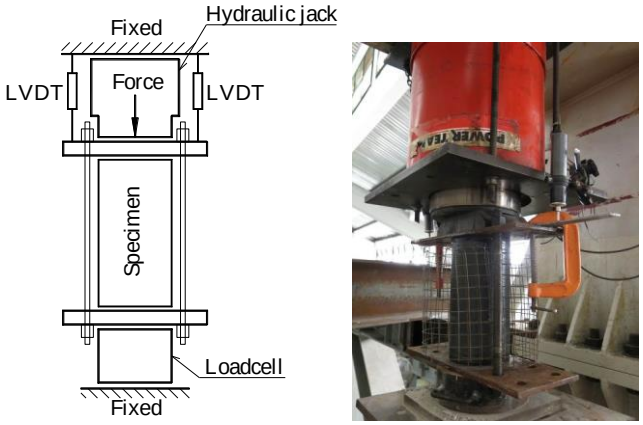

(a) Outline (b) A specimen on the testing machine

Fig. 4 Experiment setup

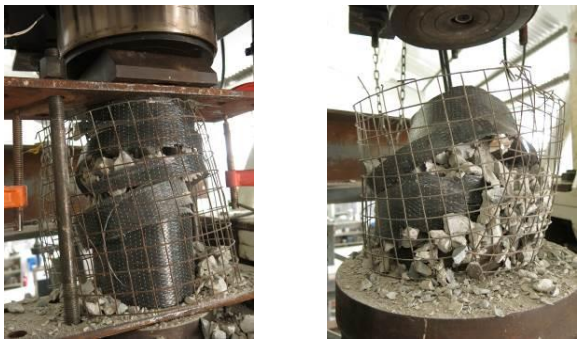

(a) A preloaded specimen (b) An un-preloaded specimen

Fig. 5 Examples of failed specimens on the testing machine

displacements during the test were automatically recorded by the data logger and computer system. The tests were terminated when the specimens completely fail by explosion.

3. Experimental results and discussions

3.1 Failure of specimens

Figs. 5(a)-(b) respectively show the typical failure of preloaded and un-preloaded specimens confined by FRP on the testing machine. Fig. 6 shows the failure of all FRP confined specimens after taking from the testing machine. These specimens were in the form of explosive failure after the FRP fracture. The location of the FRP fracture was at the mid-height of specimens. This fracture location is attributed to the higher lateral strain at the mid-height compared with that at the two specimen ends which may be affected by the friction between concrete and steel plates. The two parts of several failed specimens were in the form of conical shapes. The concrete part at middle of specimen was exploded into small particles and dust while the fracture of FRP in the middle part of specimens can be visual in Figs. 5-6. This conical form of failure may be resulted from the high confinement provided by FRP. A little fracture sound of FRP was heard when FRP was close to its rupture. The sound slightly increased until the explosion occurred; consequently, the axial load suddenly dropped to zero. The explosion is attributed to the sudden change of lateral stress from a high confinement (at ultimate load) to zero confinement (when the FRP failed). The failure of specimens is totally controlled by the failure of FRP.

3.2 Axial force-displacement curves

For each specimen, the displacements obtained from the two LVDTs were used to compute the average displacement, which was plotted versa the obtained axial compression force. Figs. 7-8 show the force-displacement curves of all FRP wrapped specimens of groups 1 and 2, respectively. These figures were plotted with the same axis system for comparison.

Based on the three force-displacement curves of each subgroup, the average force-displacement curves were computed and also plotted in Figs. 7-8. The computation of the average force-displacement curve is described as follows. Firstly, the lowest ultimate displacement of the three specimens was determined, and then this displacement domain (from 0 to the lowest ultimate displacement) was divided into several small intervals with the increment 0.01 mm. At a certain displacement, for example 0.05 mm, three forces were determined from the three force-displacement curves and then the average force of these three forces was computed. The procedure was carried out up to the lowest ultimate displacement; consequently, the average force-displacement curve of the subgroup was obtained. The average curves were plotted as the continuous lines and

(a) un-preloaded specimens

(b) Specimens with preload 20%

(c) Specimens with preload 30%

(d) Specimens with preload 40%

Fig. 6 Failure of specimens after testing

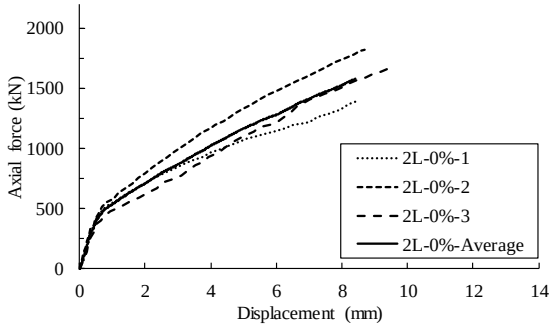

(a) 2L-0

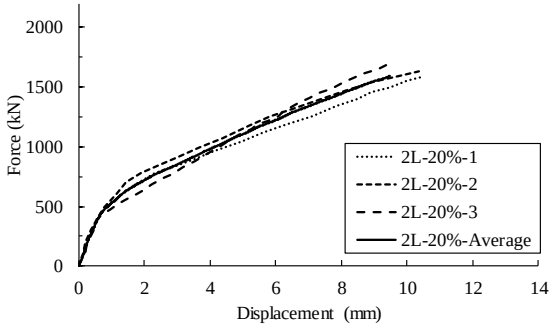

(b) 2L-20

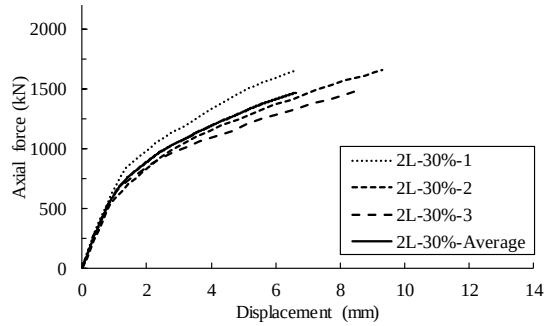

(c) 2L-30

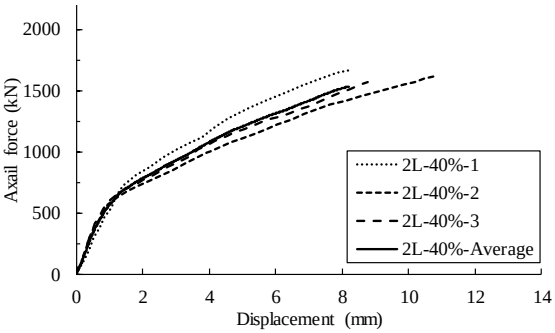

(d) 2L-40

Fig. 7 Axial force-displacement cures of group 1 specimens

were latterly used to determine the properties of specimen subgroups as presented in sections 3.3-3.6.

Overall, the behavior can be divided into two stages: elastic and plastic. For each subgroup of three specimens, the three elastic branches seem to be similar and almost identical to the average elastic branch. However, larger diversions in the plastic stage can be observed in Figs. 7-8. At the ultimate point, FRP failed, leading to the explosion of FRP confined specimens, and the axial force immediately dropped to zero. One important aspect shown by the force-deformation curves is that the elastic parts are much shorter than the plastic parts. In addition, the elastic part is under approximately 500 kN, which is close to the maximum load of plain concrete specimens.

3.3 Preload effect on elastic stiffness

The elastic stiffness was determined based on the

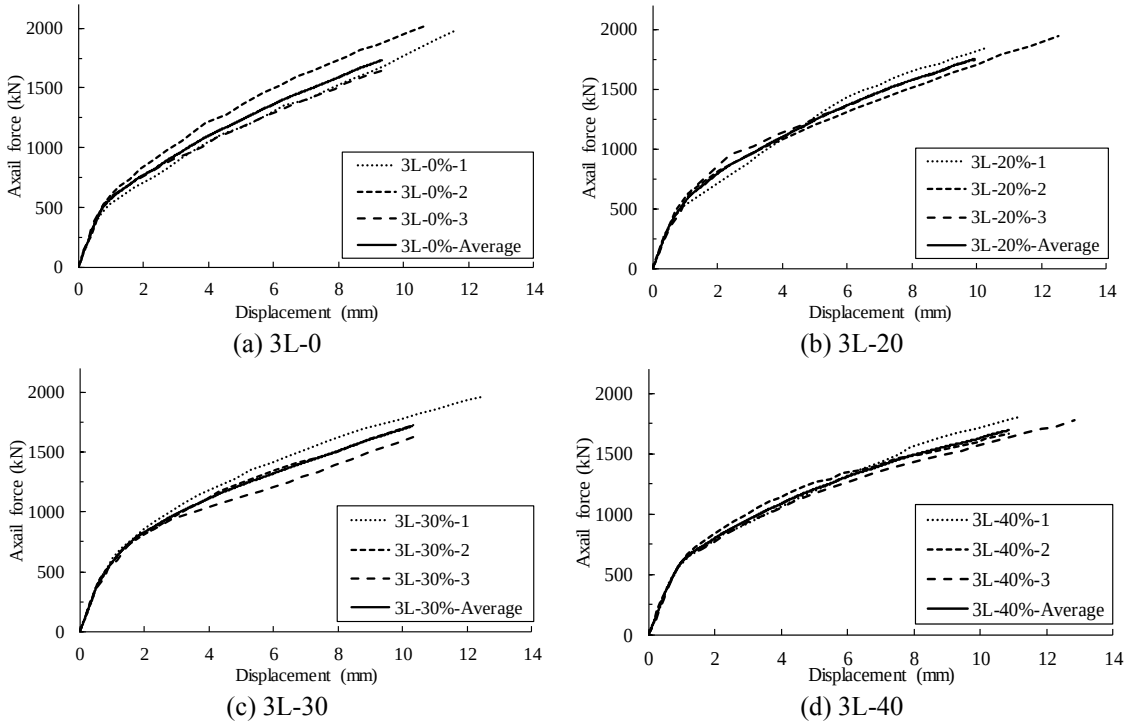

(a) 3L-0 (b) 3L-20

(c) 3L-30 (d) 3L-40

Fig. 8 Axial force-displacement curves of group 2 specimens

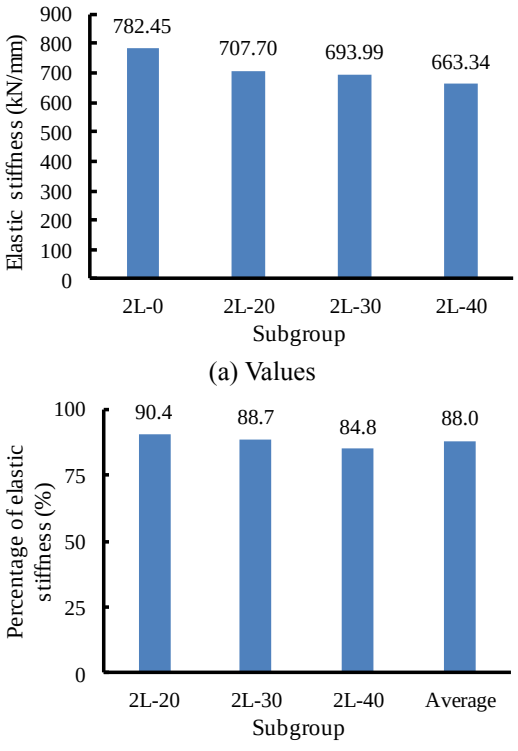

(a) Values

(b) Percentage

Fig. 9 Elastic stiffness of group 1

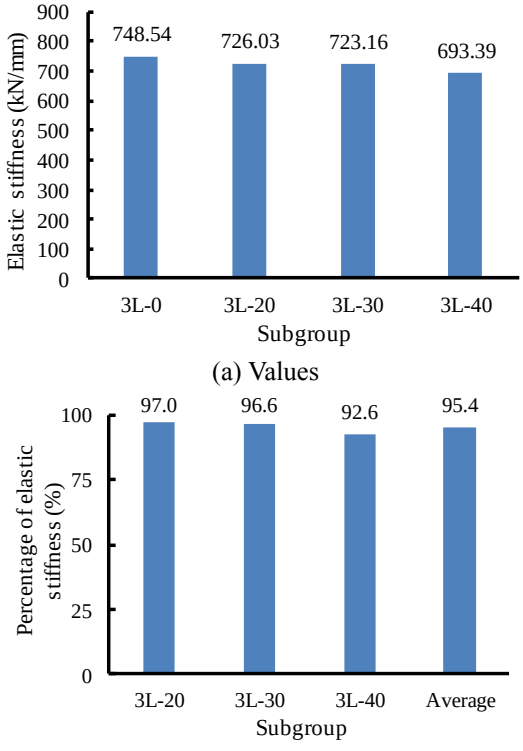

(a) Values

(b) Percentage

Fig. 10 Elastic stiffness of group 2

average force-displacement curves obtained in the section 3.2. Fig. 9(a) shows the elastic stiffness of 4 subgroups of groups 1, and a clear trend can be observed in this figure that the stiffness decreases as the preload increases. The elastic stiffness decreases from 782.45 kN/mm to 663.34 kN/mm when the preload increases from 0% to 40%. Compared with the elastic stiffness of the subgroup with zero preload (2L-0), the elastic stiffness of subgroups with the preload 20%, 30% and 40% reduced to 90.4, 88.7 and 84.8%, respectively, as shown in Fig. 9(b). The average of these values is 88.0%; thus, the elastic stiffness reduced 12.0% due to the preload.

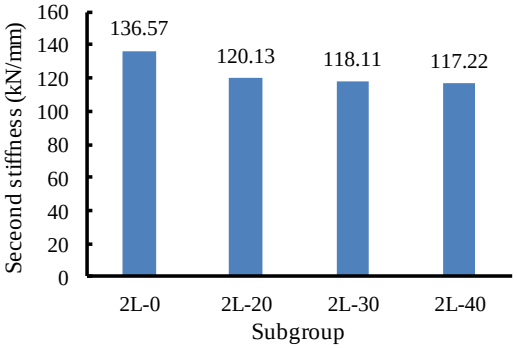

(a) Values

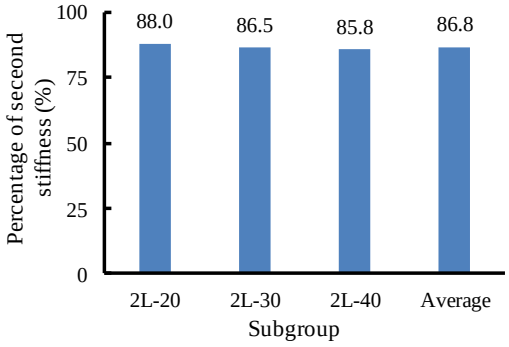

(b) Percentage

Fig. 11 Second stiffness of group 1

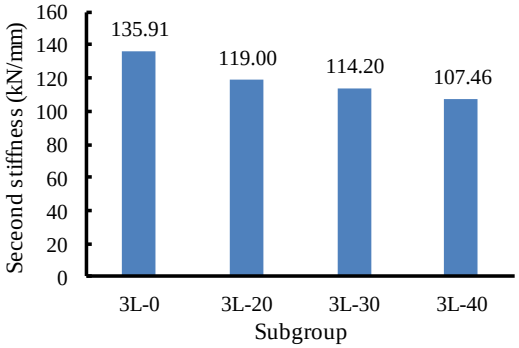

(a) Values

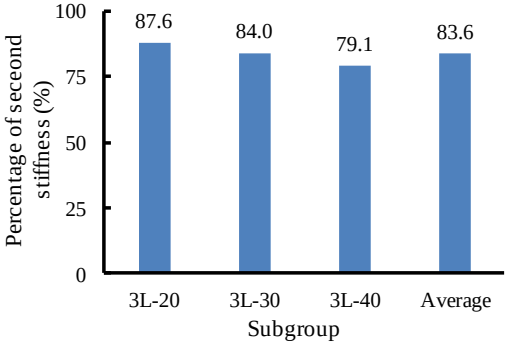

(b) Percentage

Fig. 12 Second stiffness of group 2

Similarly, Fig. 10(a) shows the values of elastic stiffness of 4 subgroups of group 2. The elastic stiffness decreases from 748.54 kN/mm to 693.39 kN/mm when the preload increases from 0% to 40%. The elastic stiffness of subgroups with the preload 20%, 30% and 40% reduced to 97.0%, 96.6% and 92.6%, respectively, when compared with that of the subgroups with zero preload as shown in Fig. 10(b). The average of these values is 95.4%; thus, the elastic stiffness reduced only 4.6% due to the preload. Compared with group 1, the number of FRP layers can mitigate the reduction of elastic stiffness due to preload. This can be attributed to the stronger confinement of 3 FRP layers than that of 2 FRP layers.

3.4 Preload effect on second stiffness

Similar to the elastic stiffness, the second stiffness was also determined based on the average force-displacement curves. Fig. 11(a) shows the second stiffness of subgroups wrapped by 2 FRP layers. The second stiffness 136.57 kN/mm of un-preloaded specimens wrapped by 2 FRP layers reduces to 120.13, 118.11 and 117.22 kN/mm when the preload is 20, 30 and 40%, respectively. Consequently, the reduction is corresponding to 88.0%, 86.5% and 85.8%, as shown in Fig. 11(b). On average the second stiffness of preloaded subgroups is 86.8% that of the un-preloaded subgroup and the preload thus reduces 13.2% the second stiffness.

Analogous to Fig. 11, Fig. 12(a) shows the second stiffness of subgroups of group 2 and Fig. 12(b) shows the percentage of the second stiffness of preloaded subgroups compared with that of the un-preloaded subgroup. A clear

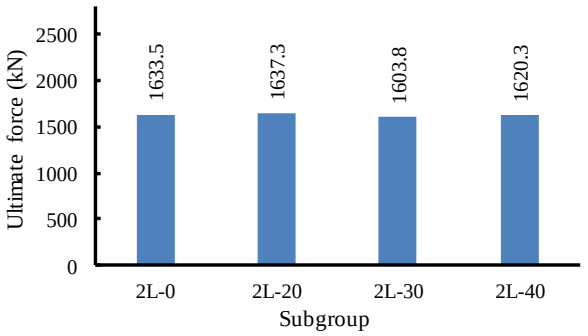

(a) Group 1

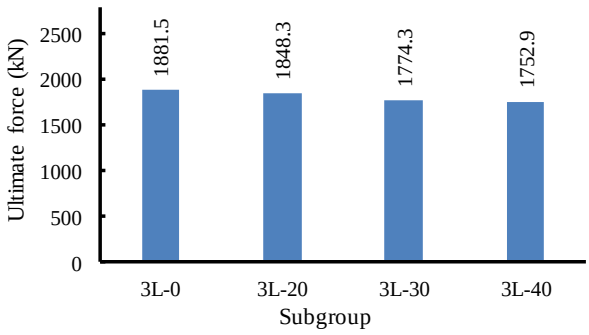

(b) Group 2

Fig. 13 Ultimate forces

trend of decrease on the second stiffness can be observed in Fig. 12. The second stiffness of the un-preloaded specimen is 135.91 kN/mm while those of the 20, 30 and 40% preloaded specimens are 119.00, 114.20 and 107.46 kN/mm, respectively, as shown in Fig. 12(a). Compared

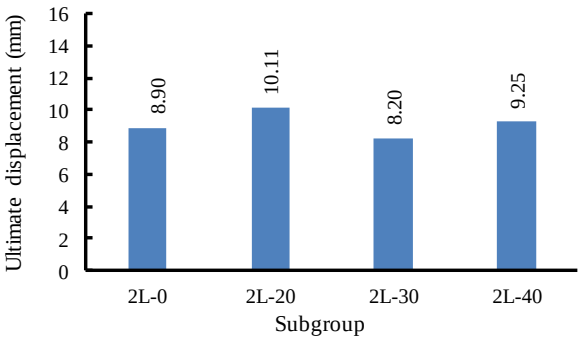

(a) Group 1

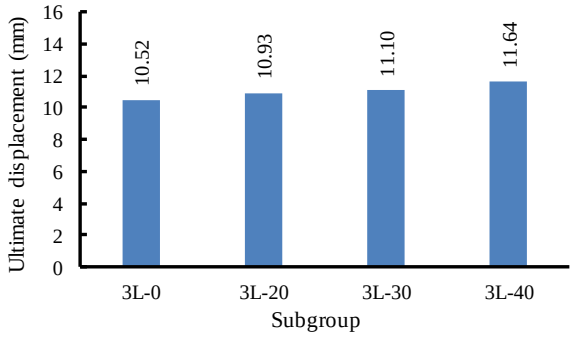

(b) Group 2

Fig. 14 Ultimate displacements

with the second stiffness of the un-preloaded subgroup 3L-0, the second stiffness reduces to 87.6%, 84.0% and 75.2%, making the average reduction 83.6% of the second stiffness. On average, the preload reduces 16.4% the second stiffness. Thus, similar to elastic stiffness, the axial preload apparently reduces the second stiffness of specimens.

3.5 Preload effect on ultimate load-carrying capacity

Figs. 13(a)-(b) show the average ultimate load-carrying capacity of groups 1 and 2, respectively. The ultimate forces of subgroups are quite close to each other. The ultimate force slightly decreases as the preload increases. The subgroup 3L-40 has the strongest reduction of ultimate force from 1881.5 kN to 1752.9 kN, corresponding to 6.8% while the reductions of other subgroups can be negligible.

3.6 Preload effect on ultimate displacement

Figs. 14(a)-(b) show the average ultimate displacements of subgroups in groups 1 and 2, respectively. The preload seems to have an unclear effect on the ultimate displacement. This is explained by the fact that the failure of FRP depends on the crack distribution in concrete. Cracks developed in concrete during the loading process can lead to stress concentration in FRP; consequently, the failure of FRP can be significantly different. The ultimate displacement of preloaded concrete confined by FRP can be a complicated issue as it involves in the random distribution of damage in concrete. Explosive failure described in Section 3.1 can be the evidence for this complicated issue. Further studies should be carried out to investigate the effect of preload on this issue of ultimate displacement.

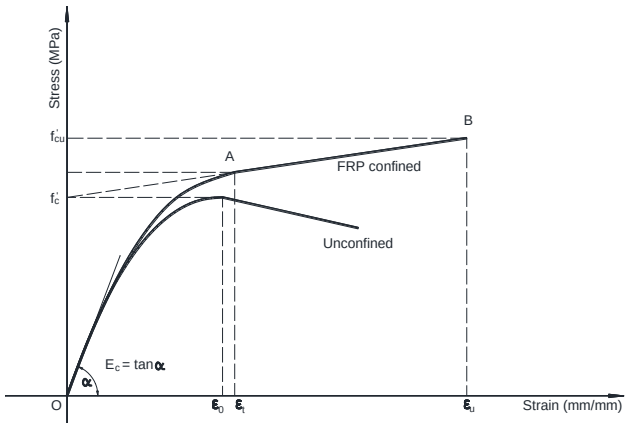

Fig. 15 Stress-strain model of FRP confined concrete proposed by Lam and Teng (2003a)

4. Comparisons with models of FRP-confined concrete

FRP wraps can significantly increase the mechanical properties of concrete, which has been widely proven by researchers (Harajli *et al.* 2006, Lam and Teng 2003a, b, Wei and Wu 2012, Wu *et al.* 2007, Youssef *et al.* 2007, and others). Amongst many models available in the literature, the Lam and Teng (2003a) model has been widely used, and this model was employed in ACI 440 code (2008) probably because it is simple but accurate and easy to use. This model is thus selected for the comparison between the results obtained from the model and those obtained from the tests of un-preload FRP confined concrete specimens. Fig. 15 shows the stress-strain model of FRP confined concrete proposed by Lam and Teng (2003a). The model is expressed by Eqs. (1)-(2), followed by Eqs. (3)-(4).

Branch OA ($0 \le \varepsilon_c \le \varepsilon_t$)

$$f_c = E_c\varepsilon_c - \frac{(E_c - E_2)^2}{4f_c^{'}}\varepsilon_c^2 \quad (1)$$

Branch AB ($\varepsilon_t \le \varepsilon_c \le \varepsilon_u$)

$$f_c = f_c^{'} + E_2\varepsilon_c \quad (2)$$

$$\varepsilon_t = \frac{2f_c^{'}}{E_c - E_2} \quad (3)$$

$$E_2 = \frac{f_{cu}^{'} - f_c^{'}}{\varepsilon_u} \quad (4)$$

where E_2 is the slope of the second branch; $f_{cu}^{'}$ is the compressive strength of confined concrete; ε_u is the ultimate strength of confined concrete. The parameters for the model proposed by Lam and Teng (2003a) and these parameters in ACI 440 code (2008) are different as compared in the following. It is noted that this comparison is for circular cross-section confined by CFRP.

Regarding the ultimate stress $f_{cu}^{'}$, Eqs. (5)-(6), followed by Eq. (7), are widely accepted. In these equations, t_f is the total thickness of the FRP wraps, E_f is the

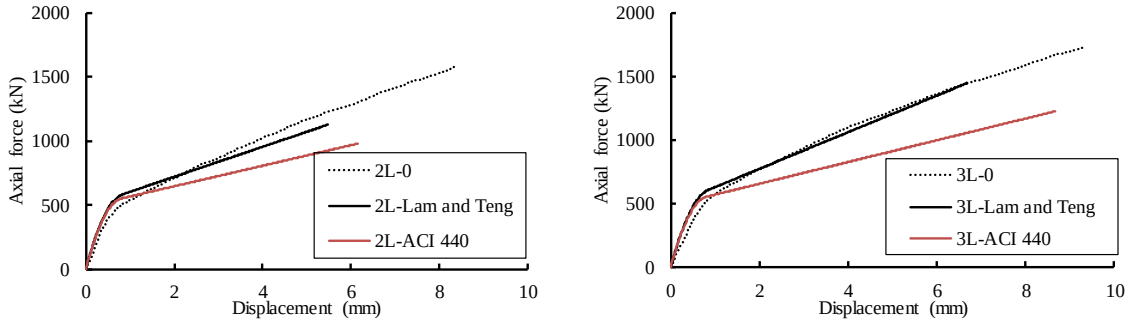

(a) Group 1 (b) Group 2

Fig. 16 Comparisons of force-displacement curves of un-preload specimens and Lam and Teng (2003a) model

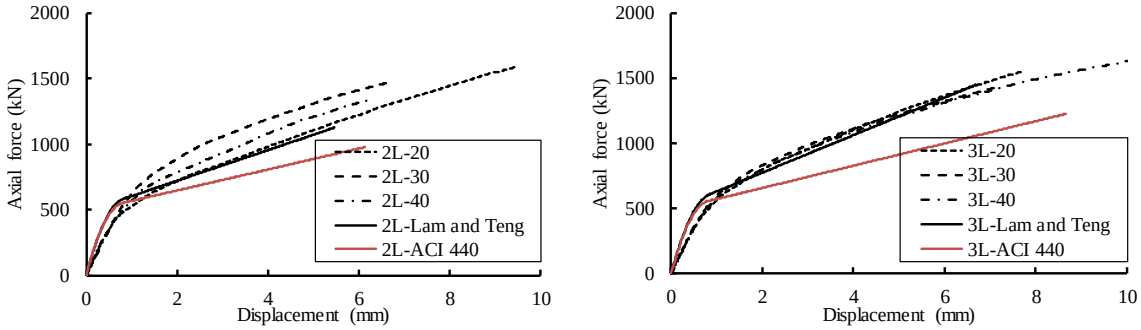

(a) Group 1 (b) Group 2

Fig. 17 Comparison the force-displacement curves of preload specimens and Lam and Teng (2003a) and ACI 440 (2008) models

FRP modulus, and D=2R is the diameter of cylinder specimen. In ACI 440 code (2008), the second term of the Eq. (5) is multiplied by the additional reduction factor ψ_f=0.95, and the threshold value 0.08, instead of 0.07, is used.

$$f_{cu}^{'} = f_c^{'}\left[1+3.3\frac{f_{la}}{f_c^{'}}\right] \quad \text{if} \quad \frac{f_{la}}{f_c^{'}} \geq 0.07 \tag{5}$$

$$f_{cu}^{'} = f_c^{'} \quad \text{if} \quad \frac{f_{la}}{f_c^{'}} < 0.07 \tag{6}$$

$$f_{la} = \frac{E_f t_f}{R}\varepsilon_{h,rup} = \frac{2E_f t_f}{D}\varepsilon_{h,rup} \tag{7}$$

Regarding the ultimate strain ε_u, different models have been proposed in the literature as presented in Table 2. It is noted that these models of ultimate strain are of circular cross section and are presented in chronological order. In these strain models, $\varepsilon_{h,rup}$=k_ε ε_{frp} is the rupture strain of FRP; k_ε is 'FRP strain efficiency factor'; ε_{frp} is the rupture strain of FRP coupon specimens; v_c is the Poisson's ratio of concrete; E_j=2$E_f t_f$/D is the jacket lateral stiffness.

For CFRP, the strain efficiency factor k_ε have been recommended to be 0.586 by Lam and Teng (2003a) based on 52 CFRP wrapped specimens and 0.55 by ACI 440 (2008). Later, based on 62 test results, Realfonzo and Napoli (2013) recommended the value 0.63 which is close to the average value 0.62 (for both CFRP and GFRP) recommended by Baji (2017) using 661 FRP (477 CFRP and 184 GFRP) confined cylinders collected from literature.

Table 2 Models of ultimate strain

Model of ultimate strain	Reference
$\varepsilon_u = \varepsilon_o\left[1.75+12\frac{f_{la}}{f_c^{'}}\left(\frac{\varepsilon_{h,rup}}{\varepsilon_o}\right)^{0.45}\right]$	Lam and Teng (2003a)
$\varepsilon_u = \varepsilon_o\left[1.5+12\frac{f_{la}}{f_c^{'}}\left(\frac{\varepsilon_{h,rup}}{\varepsilon_o}\right)^{0.45}\right]$	ACI 440 code (2008)
$\varepsilon_u = \varepsilon_o\left[1.00+\sqrt{2}\left(\frac{\varepsilon_{h,rup}}{\varepsilon_o}-v_c\right)\left(\frac{E_j}{f_c^{'2}}\right)^{2/3}\right]$	Berthet *et al.* (2006)
$\varepsilon_u = \varepsilon_o\left[1.00+\frac{1}{5.9}\left(\frac{\varepsilon_{h,rup}}{\varepsilon_o}-v_c\right)\left(\frac{E_j}{f_c^{'}}\right)^{0.65}\right]$	Tamuzs *et al.* (2006)
$\varepsilon_u = \varepsilon_o\left[1.75+6.5\left(\frac{\varepsilon_{h,rup}}{\varepsilon_o}\right)^{1.45}\left(\frac{E_j}{f_c^{'}/\varepsilon_o}\right)^{0.80}\right]$	Teng *et al.* (2009)
$\varepsilon_u = \varepsilon_o\left[c_2+0.271\left(\frac{E_j}{f_c^{'}}\right)^{0.90}\left(\frac{\varepsilon_{h,rup}^{1.35}}{\varepsilon_o}\right)\right]$; $c_2 = 2-\frac{f_c^{'}-20}{100}\geq 1.0$	Ozbakkaloglu and Lim (2013)
$\varepsilon_u = \varepsilon_o\left[1.00+\frac{1}{5.1}\left(\frac{\varepsilon_{h,rup}}{\varepsilon_o}\right)\left(\frac{E_j}{f_c^{'}}\right)^{0.56}\right]$	Baji *et al.* (2016)

The most updated value k_ε for CFRP is 0.68 which was computed by Baji *et al*. (2016) based on the largest database of 509 CFRP wrapped specimens, and this value is thus used in this current paper.

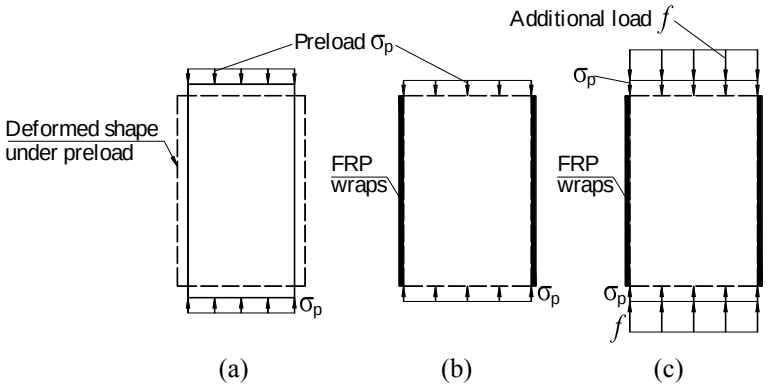

Fig. 18 Stages of concrete under preload and FRP confinement

Amongst the strain models presented in Table 2, Baji *et al.* (2016) model is the most updated and was proposed based on an extensive statistic data collected from different publications available in the literature. Therefore, this strain model is selected to use in this paper. In addition, the model in ACI 440 (2008) was also employed for comparison in order to have a view on design codes.

Using the material properties obtained in section 2.1, the stress-strain curve based on Lam and Teng (2003a) model with the ultimate strain model proposed by Baji *et al.* (2016) was computed and then converted into force-displacement curve. The average force-displacement curves of subgroups 2L-0 and 3L-0 are respectively compared with the curve obtained using Lam and Teng (2003a) model for cylinder specimens wrapped by 2 and 3 FRP layers, as shown in Figs. 16(a)-(b), respectively. It can be seen in these figures that the two results show an overall good approximation while ACI 440 (2008) underestimates the plastic part which can be appropriate for safe design.

Although the Lam and Teng (2003a) model and ACI 440 (2008) do not take into account the preload effects, they are worth comparing with the tests of preloaded FRP confined specimens, aiming at analysing the preload effects. Figs. 17(a)-(b) show the comparisons of the results obtained from the above models and those of groups 1 and 2. The plastic portions are quite close to each other while the elastic portions of the model are overestimated because these models do not take into account the preload effects. This difference is kept in mind for the modification of the Lam and Teng (2003a) model to include the preload effects presented in section 5.

5. Mechanism and the modified model of FRP confined concrete with preload

5.1 Mechanism

A plain concrete specimen subjected to preload experiences three stages of deformation as illustrated in Fig. 18. The specimen is firstly subjected to preload and deformed as shown in Fig. 18(a). Then, this deformed specimen (specimen with preload) is wrapped by FRP layers as shown in Fig. 18(b). Finally, the specimen is additionally loaded to failure as shown in Fig. 18(c), and

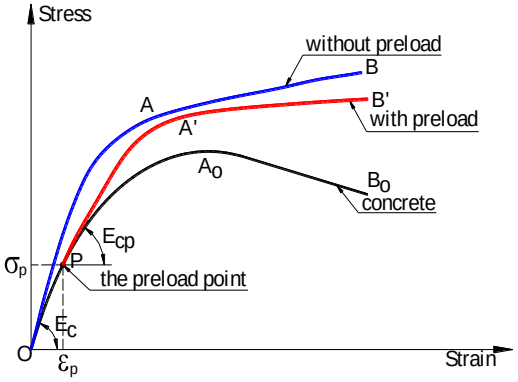

Fig. 19 Mechanism of preload effects on the elastic stiffness

FRP works only in this stage of additional loading.

Fig. 19 illustrates the mechanism of preload effects on the mechanical behaviour of FRP confined concrete. The stress-strain behaviour of plain concrete is plotted as the 'black' curve OA_oB_o. The 'blue' curve OAB illustrates the behaviour of un-preloaded concrete confined by FRP, which is started from the origin O (zero strain and stress), at which the slope is the original elastic modulus of plain concrete. This 'blue' curve is well expressed by models available in the literature such as Lam and Teng (2003a) model. However, the important factor that critically affects the behaviour of preloaded concrete confined by FRP is the slope at the preload when FRP is applied. The preload changes the mechanical behaviour of preloaded confined FRP concrete, which is illustrated by the 'red' curve PA'B'. This 'red' curve started at the preload point P, whose slope is much smaller than the slope at the origin (the original elastic modulus of concrete). The difference of the starting points O and P when FRP is applied consequently leads to the difference of the 'red' and 'blue' curves. The stress-strain curves of FRP confined specimens with preload can be expressed by two parts: 1) the part OP which is of the plain concrete from zero to the strain at preload ε_p, and 2) the part PA'B' which is the 'red' curve from P to the ultimate ($\varepsilon_p \leq \varepsilon_c \leq \varepsilon_u$). This 'red' curve starts from the point P; therefore, the modulus E_{cp} which is the slope at P, instead of E_c which is the original modulus, is used for the model of FRP confined concrete. Instead of confining the concrete with the mechanical property expressed by the curve OA_oB_o, FRP is now confining the concrete with the

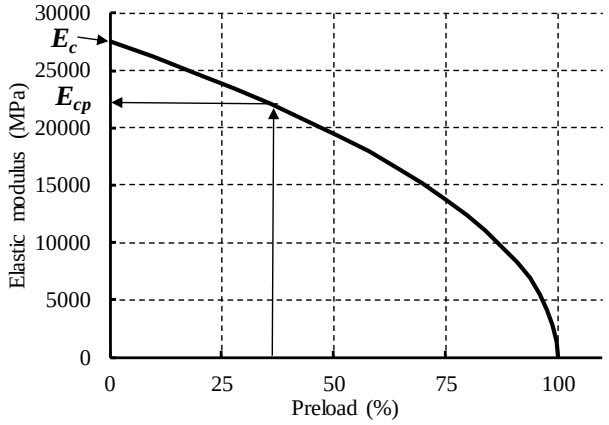

Fig. 20 Variation of modulus with respected to the preload ($f_c^{'}$=27.56 MPa)

mechanical property expressed by the curve PA_oB_o. This is the reason for changes of mechanical properties of FRP confined concrete with preload compared with those without preload.

The stress-strain behaviour of plain concrete can be expressed by Hognestad (1951) model which includes two branches (the parabola branch OA_o and the descending branch A_oB_o) as shown in Fig. 19. The ascending branch OA_o is a parabola described by Eq. (8), where ε_c is the strain; ε_o is the strain at maximum stress expressed by Eq. (9); $f_c^{'}$ is the maximum stress of concrete and E_c is the modulus of elasticity. The descending branch A_oB_o (after the maximum stress) expresses the linear relationship between stress and strain. The stress reduces 15% comparing to $f_c^{'}$ when the strain reaches its ultimate value of 0.0038.

$$f_c = f_c^{'}\left[\frac{2\varepsilon_c}{\varepsilon_o}-\left(\frac{\varepsilon_c}{\varepsilon_o}\right)^2\right] \quad \text{if} \quad 0 \le \varepsilon_c \le \varepsilon_o \tag{8}$$

$$\varepsilon_o = \frac{2f_c^{'}}{E_c} \tag{9}$$

The modulus at a specific preload (corresponding to a specific strain) is the slope of the stress-strain curve OA_o (Fig. 19) and is computed by taking the first derivative of the Eq. (8) with respect to the strain ε_c, as shown in Eq. (10).

$$E_{cp} = Slope = f_c^{'}\left[\frac{2}{\varepsilon_o}-\frac{2\varepsilon_c}{\varepsilon_o^2}\right] \tag{10}$$

The Eq. (10) can be applied for any preload percentage varying from zero to 100% the maximum stress of concrete. When the preload is zero (ε_c=0), the modulus or the slope computed using Eq. (10) is $E_c = 2f_c^{'}/\varepsilon_o$, which is the same as the modulus in the Hognestad (1951) model as shown in Eq. (9). When the preload exists, using the original modulus of concrete E_c to substitute into the Lam and Teng (2003a) model is obviously incorrect. The modulus used to substitute should be the slope corresponding to the strain at the preload, which is expressed in Eq. (10). This value is apparently smaller than the original elastic modulus of concrete. Fig. 20 shows a variation example of concrete modulus (the slope) with respected to the preload, expressed by Eq. (10). It can be seen that the modulus decreases significantly as the preload increases. The elastic modulus E_c is the largest value when concrete is without preload, and it reduces to zero when the preload is 100%.

5.2 The proposed modification for the stress-strain model

Based on the mechanism analysed and presented in Section 5.1, a model for FRP confined concrete with preload should ideally include three branches as follows:

Branch OP ($0 \le \varepsilon_c \le \varepsilon_p$): the model of plain concrete applied for the strain varying from 0 to the strain ε_p at preload. After that, the model of FRP confined concrete without preload can be applied to the specimen with the initial condition at P, which is corresponding to the preload stress σ_p and the preload strain ε_p, instead of the initial condition at zero. In other words, the Lam and Teng (2003a) model can be applied for concrete with the properties described by the stress-strain curve from P onward (the curve PA_oB_o), not from O as for unpreload concrete (see Fig. 19). Therefore, the maximum compressive stress $f_c^{'}$ in the Lam and Teng (2003a) model should be subtracted by the preload stress σ_p or $pf_c^{'}$, in which p is the preload ratio. In other words, $f_{cp}^{'} = f_c^{'}(1-p)$, instead of $f_c^{'}$, is used. Similarly, the strain ε_c is also subtracted by the strain at preload ε_p. Importantly, the modulus of concrete at the preload E_{cp} should be used in the Lam and Teng (2003a) model, instead of E_c. Consequently, the Lam and Teng (2003a) model is modified for the branches OA and AB to become the branches *PA'* and *A'B'* (Fig. 19) as follows:

Branch PA' ($\varepsilon_p \le \varepsilon_c \le \varepsilon_t$)

$$f_c = f_{cp} + E_{cp}\left(\varepsilon_c - \varepsilon_p\right) - \frac{\left(E_{cp}-E_2\right)^2}{4f_{cp}^{'}}\left(\varepsilon_c-\varepsilon_p\right)^2 \tag{11}$$

Branch A'B' ($\varepsilon_t \le \varepsilon_c \le \varepsilon_u$)

$$f_c = f_{cp} + f_{cp}^{'} + E_2\left(\varepsilon_c - \varepsilon_p\right) \tag{12}$$

$$\varepsilon_t = \frac{2f_{cp}^{'}}{E_{cp}-E_2} \tag{13}$$

$$E_2 = \frac{f_{cup}^{'} - f_{cp}^{'}}{\varepsilon_u - \varepsilon_p} \tag{14}$$

$$f_{cup}^{'} = f_{cp}^{'}\left[1+3.3\frac{f_{la}}{f_{cp}^{'}}\right] \quad \text{if} \quad \frac{f_{la}}{f_{cp}^{'}} \ge 0.07 \tag{15}$$

$$f_{cu}^{'} = f_{cp}^{'} \quad \text{if} \quad \frac{f_{la}}{f_{cp}^{'}} < 0.07 \tag{16}$$

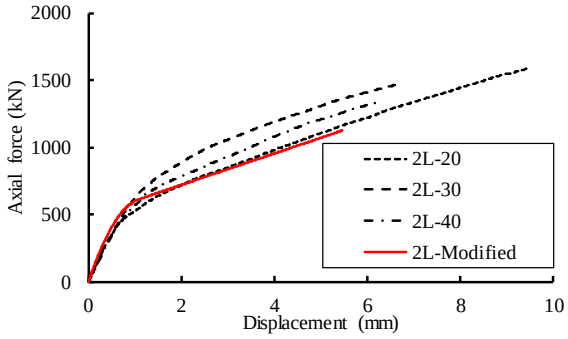

(a) Group 1

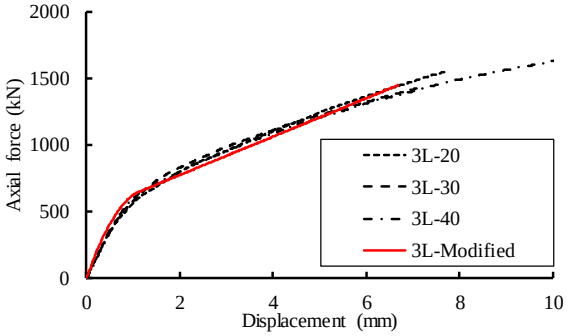

(b) Group 2

Fig. 21 Modified Lam and Teng (2003a) model for preloaded FRP confined concrete

$$\varepsilon_u = \left(\varepsilon_o - \varepsilon_p\right)\left[1.75 + 5.53\frac{f_{la}}{f_{cp}^{'}}\left(\frac{\varepsilon_{h,rup}}{\varepsilon_o - \varepsilon_p}\right)^{0.45}\right] \quad (17)$$

$$f_{la} = \frac{E_f t_f}{R}\varepsilon_{h,rup} = \frac{2E_f t_f}{D}\varepsilon_{h,rup} \quad (18)$$

The above modification follows the mechanism described in section 5.1 and obviously it needs to be improved; however, the model becomes cumbersome and difficult to use for structural engineers because it includes three branches and involves in several parameters. For simplification, the branch OP and PA' is merged to become one branch starting from O. In addition, the modulus of concrete at preload is used while effects of parameters such as the preload stress and strain are ignored. When the modulus of concrete at preload E_{cp} described in Eq. (10) is employed in the Lam and Teng (2003a) model, the obtained results are shown in Fig. 21. As can be seen, the results obtained from the modified Lam and Teng (2003a) model show a good agreement with the experimental results.

6. Conclusions

In this paper, experiments on 27 cylinder concrete specimens with the diameter 150 mm and the height 300 mm were conducted. Three of these specimens were used to determine the maximum load sustained by plain concrete specimens while the other 24 specimens were used to investigate the preload effects on FRP-confined concrete. These 24 specimens were divided into 8 subgroups, which were firstly subjected to preloads 0%, 20%, 30% and 40% the maximum load of plain concrete and then wrapped by 2 and 3 FRP layers. After preloading and FRP wrapping, all specimens were tested under axial compression to failure. The following conclusions are drawn based on the obtained results:

- Explosive failure is a characteristic of the tested specimens and is governed by the rupture of FRP. The failure modes of FRP-confined concrete specimens are in the form of conical shapes which are resulted from the high confinement of FRP. The tested specimens are completely unable to carry load when the explosive failure occurs.
- The elastic stiffness decreases when the preload increases. On average, the preload decreases 12.0% the elastic stiffness when specimens were wrapped by 2 FRP layers. The increase of number of FRP layers can mitigate the loss of the elastic stiffness due to the preload effects, by reducing only 4.6% as evidenced by preloaded specimens wrapped by 3 FRP layers.
- The second stiffness also decreases as the preload increases. On average, the preload decreases 13.2% and 16.4% the second stiffness when the specimens were wrapped by 2 and 3 FRP layers, respectively.
- The preload has a marginal effect on the ultimate load-carrying capacity of FRP confined concrete while it unclearly affects the ultimate displacement. These effects are attributed to the fact that the failure of preloaded FRP confined concrete specimens is governed by the rupture of FRP which heavily depends on the cracks which randomly developed in concrete, leading to stress concentration in FRP.
- Mechanism of the preload effects on mechanical behaviour of FRP confined concrete was presented, providing information to develop stress-strain models of preloaded FRP confined concrete. Based on this mechanism, the modification to the Lam and Teng (2003a) model is proposed to take into account the preload effects on behaviour of FRP confined concrete. Although this modification aims at simply practical use for structural engineers, the modified model demonstrates a reasonable accuracy.

Acknowledgements

This research is funded by Ho Chi Minh city University of Technology-VNU-HCM under grant number T-KTXD-2019-16.

The author would like to express special thanks to staffs in the Laboratory of Structural Engineering and Laboratory of Mechanics of Materials and Structures, Department of Civil Engineering, Ho Chi Minh city University of Technology (HCMUT)-Vietnam National University for their help and encouragement. The author also thanks Dr. Hung The Dinh, Carboneering company Ltd. (www.carboneering.com), for providing CFRP material which was used for the experiment. The authors would like to express thanks to workers for their help on physical work with reasonable payment.

References

Abdel-Kareem, A.H. (2014), "Shear strengthening of reinforced concrete beams with rectangular web openings by FRP Composites", *Adv. Concrete Constr.*, **2**(4), 281-300. https://doi.org/10.12989/acc.2014.2.4.281.

ACI (2008), Guide for the Design and Construction of Externally Bonded FRP Systems for Strengthening Concrete Structures (ACI 440.2R-08).

Ahmad, H., Hameed, R., Riaz, M.R. and Gillani, A.A. (2018), "Strengthening of concrete damaged by mechanical loading and elevated temperature", *Adv. Concrete Constr.*, **6**(6), 645-658. https://doi.org/10.12989/acc.2018.6.6.645.

Baji, H. (2017), "Calibration of the FRP resistance reduction factor for FRP-confined reinforced concrete building columns", *J. Compos. Constr.*, **21**(3), 04016107. https://doi.org/10.1061/(ASCE)CC.1943-5614.0000769.

Baji, H., Ronagh, H.R. and Li, C.Q. (2016), "Probabilistic design models for ultimate strength and strain of FRP-confined concrete", *J. Compos. Constr.*, **20**(6), 04016051. https://doi.org/10.1061/(ASCE)CC.1943-5614.0000704.

Balsamo, A., Colombo, A., Manfredi, G., Negro, P. and Prota, A. (2005), "Seismic behavior of a full-scale RC frame repaired using CFRP laminates", *Eng. Struct.*, **27**, 769-780. https://doi.org/10.1016/j.engstruct.2005.01.002.

Berthet, J.F., Ferrier, E. and Hamelin, P. (2006), "Compressive behavior of concrete externally confined by composite jackets: Part B: modeling", *Constr. Build. Mater.*, **20**(5), 338-347. https://doi.org/10.1016/j.conbuildmat.2005.01.029.

Cao, V.V. and Pham, S.Q. (2019), "Comparison of CFRP and GFRP wraps on reducing seismic damage of deficient reinforced concrete structures", *Int. J. Civil Eng.*, **17**(11), 1667-1681. https://doi.org/10.1007/s40999-019-00429-y.

Cao, V.V. and Ronagh, H.R. (2014), "Reducing the seismic damage of reinforced concrete frames using FRP confinement", *Compos. Struct.*, **118**, 403-415. https://doi.org/10.1016/j.compstruct.2014.07.038.

Eslami, A. and Ronagh, H.R. (2013), "Effect of FRP wrapping in seismic performance of RC buildings with and without special detailing-A case study", *Compos. Part B: Eng.*, **45**(1), 1265-1274. https://doi.org/10.1016/j.compositesb.2012.09.031.

Ferrotto, M.F., Fischer, O. and Cavaleri, L. (2018), "Analysis-oriented stress-strain model of CRFP-confined circular concrete columns with applied preload", *Mater. Struct.*, **51**(2), 44. https://doi.org/10.1617/s11527-018-1169-0.

Garcia, R., Hajirasouliha, I. and Pilakoutas, K. (2010), "Seismic behaviour of deficient RC frames strengthened with CFRP composites", *Eng. Struct.*, **32**, 3075-3085. https://doi.org/10.1016/j.engstruct.2010.05.026.

Harajli, M.H. and Rteil, A.A. (2004), "Effect of confinement using fiber-reinforced polymer or fiber-reinforced concrete on seismic performance of gravity load-designed columns", *ACI Struct. J.*, **101**(1), 47-56.

Harajli, M.H., Hantouche, E. and Soudki, K. (2006), "Stress-strain model for fiber-reinforced polymer jacketed concrete columns", *ACI Struct. J.*, **103**(5), 672-682.

Hognestad, E. (1951), "A study of combined bending axial load in reinforced concrete members", Bulletin Series No. 399, **49**, Engineering Experimental Station, The University of Illinois., Urbana.

Hosseinpour, F. and Abbasnia, R. (2014), "Experimental investigation of the stress-strain behavior of FRP confined concrete prisms", *Adv. Concrete Constr.*, **2**(3), 177-192. https://doi.org/10.12989/acc.2014.2.3.177.

Hosseinpour, F. and Abdelnaby, A.E. (2015), "Statistical evaluation of the monotonic models for FRP confined concrete prisms", *Adv. Concrete Constr.*, **3**(3), 161-185. https://doi.org/10.12989/acc.2015.3.3.161.

Lam, L. and Teng, J.G. (2003a), "Design-oriented stress-strain model for FRP-confined concrete", *Constr. Build. Mater.*, **17**, 471-489. https://doi.org/10.1016/S0950-0618(03)00045-X.

Lam, L. and Teng, J.G. (2003b), "Design-oriented stress-strain model for FRP-confined concrete in rectangular columns", *J. Reinf. Plast. Compos.*, **22**(13), 1149-1186. https://doi.org/10.1177/0731684403035429.

Lao, X., Han, X., Ji, J. and Chen, B. (2019), "The compression behavior of CFRP-repaired damaged square RC columns", *Constr. Build. Mater.*, **223**, 1154-1166. https://doi.org/10.1016/j.conbuildmat.2019.07.182.

Ludovico, M.D., Manfredi, G., Mola, E., Negro, P. and Prota, A. (2008a), "Seismic behavior of a full-scale RC structure retrofitted using GFRP laminates", *J. Struct. Eng.*, **134**(5), 810-821. https://doi.org/10.1061/(ASCE)0733-9445(2008)134:5(810).

Ludovico, M.D., Prota, A., Manfredi, G. and Cosenza, E. (2008b), "Seismic strengthening of an under-designed RC structure with FRP", *Earthq. Eng. Struct. Dyn.*, **37**, 141-162. https://doi.org/10.1002/eqe.749.

Mesbah, H.A. and Benzaid, R. (2017), "Damage-based stress-strain model of RC cylinders wrapped with CFRP composites", *Adv. Concrete Constr.*, **5**(5), 539-561. https://doi.org/10.12989/acc.2017.5.5.539.

Mortezaei, A., Ronagh, H.R. and Kheyroddin, A. (2010), "Seismic evaluation of FRP strengthened RC buildings subjected to near-fault ground motions having fling step", *Compos. Struct.*, **92**, 1200-1211. https://doi.org/10.1016/j.compstruct.2009.10.017.

Norris, T., Saadatmanesh, H. and Ehsani, M.R. (1997), "Shear and flexural strengthening of R⁄C beams with carbon fiber sheets", *J. Struct. Eng.*, **123**(7), 903-911. https://doi.org/10.1061/(ASCE)0733-9445(1997)123:7(903).

Ozbakkaloglu, T. and Lim, J.C. (2013), "Axial compressive behavior of FRP-confined concrete: Experimental test database and a new design-oriented model", *Compos. Part B: Eng.*, **55**, 607-634. https://doi.org/10.1016/j.compositesb.2013.07.025.

Ozcan, O., Binici, B., Canbay, E. and Ozcebe, G. (2010), "Repair and strengthening of reinforced concrete columns with CFRPs", *J. Reinf. Plast. Compos.*, **29**(22), 3411-3424. https://doi.org/10.1177/0731684410376332.

Pan, Y., Guo, R., Li, H., Tang, H. and Huang, J. (2017a), "Analysis-oriented stress-strain model for FRP-confined concrete with preload", *Compos. Struct.*, **166**, 57-67. https://doi.org/10.1016/j.compstruct.2017.01.007.

Pan, Y., Rui, G., Li, H., Tang, H. and Xu, L. (2017b), "Study on stress-strain relation of concrete confined by CFRP under preload", *Eng. Struct.*, **143**, 52-63. https://doi.org/10.1016/j.engstruct.2017.04.004.

Papanikolaou, V.K., Stefanidou, S.P. and Kappos, A.J. (2013), "The effect of preloading on the strength of jacketed R/C columns", *Constr. Build. Mater.*, **38**, 54-63. https://doi.org/10.1016/j.conbuildmat.2012.07.100.

Rahai, A. and Akbarpour, H. (2014), "Experimental investigation on rectangular RC columns strengthened with CFRP composites under axial load and biaxial bending", *Compos. Struct.*, **108**(0), 538-546. https://doi.org/10.1016/j.compstruct.2013.09.015.

Realfonzo, R. and Napoli, A. (2013), "Confining concrete members with FRP systems: Predictive vs design strain models", *Compos. Struct.*, **104**, 304-319. https://doi.org/10.1016/j.compstruct.2013.04.031.

Richard Liew, J.Y. and Xiong, D.X. (2009), "Effect of preload on the axial capacity of concrete-filled composite columns", *J. Constr. Steel Res.*, **65**(3), 709-722. https://doi.org/10.1016/j.jcsr.2008.03.023.

Saadatmanesh, H., Ehsani, M.R. and Jin, L. (1997), "Repair of earthquake-damaged RC columns with FRP wraps", *ACI Struct. J.*, **94**(2), 206-215.

Sathwik, M.C., Prashanth, M.H., Naik, S.C. and Satish, A. (2019), "Experimental and numerical studies on compressive behaviour of CFRP wrapped cylindrical concrete specimens subjected to different pre-loading conditions", *Mater. Today: Proc*., **27**(1), 327-335. https://doi.org/10.1016/j.matpr.2019.11.041.

Sheikh, S.A. and Yau, G. (2002), "Seismic behavior of concrete columns confined with steel and fiber-reinforced polymers", *ACI Struct. J.*, **99**(1), 72-80.

Sumathi, A. and Arun, V.S. (2017), "Study on behavior of RCC beams with externally bonded FRP members in flexure", *Adv. Concrete Constr.*, **5**(6), 625-638. https://doi.org/10.12989/acc.2017.5.6.625.

Takeuti, A.R., de Hanai, J.B. and Mirmiran, A. (2008), "Preloaded RC columns strengthened with high-strength concrete jackets under uniaxial compression", *Mater. Struct.*, **41**(7), 1251-1262. https://doi.org/10.1617/s11527-007-9323-0.

Tamuzs, V., Tepfers, R., Zile, E. and Ladnova, O. (2006), "Behavior of concrete cylinders confined by a carbon composite 3. Deformability and the ultimate axial strain", *Mech. Compos. Mater.*, **42**(4), 303-314. https://doi.org/10.1007/s11029-006-0040-5.

Teng, J.G., Jiang, T., Lam, L. and Luo, Y.Z. (2009), "Refinement of a design-oriented stress-strain model for FRP-confined concrete", *J. Compos. Constr.*, **13**(4), 269-278. https://doi.org/10.1061/(ASCE)CC.1943-5614.0000012.

Vandoros, K.G. and Dritsos, S.E. (2006), "Axial preloading effects when reinforced concrete columns are strengthened by concrete jackets", *Prog. Struct. Eng. Mater.*, **8**(3), 79-92. https://doi.org/10.1002/pse.215.

Vandoros, K.G. and Dritsos, S.E. (2008), "Concrete jacket construction detail effectiveness when strengthening RC columns", *Constr. Build. Mater.*, **22**(3), 264-276. https://doi.org/10.1016/j.conbuildmat.2006.08.019.

Wei, Y.Y. and Wu, Y.F. (2012), "Unified stress-strain model of concrete for FRP-confined columns", *Constr. Build. Mater.*, **26**, 381-392. https://doi.org/10.1016/j.conbuildmat.2011.06.037.

Wu, G., Wu, Z.S. and Lü, Z.T. (2007), "Design-oriented stress-strain model for concrete prisms confined with FRP composites", *Constr. Build. Mater.*, **21**(5), 1107-1121. https://doi.org/10.1016/j.conbuildmat.2005.12.014.

Youssef, M.N., Feng, M.Q. and Mosallam, A.S. (2007), "Stress-strain model for concrete confined by FRP composites", *Compos. Part B: Eng.*, **38**(5-6), 614-628. https://doi.org/10.1016/j.compositesb.2006.07.020 .

CC